A Study of Hentenna : Analysis, Simulation, Construction and Antenna Pattern Measurements

E.A. Babli, N.I. Yannopoulou, P.E. Zimourtopoulos *

[1] Independent Researcher, Thessaloniki, Greece
[2, 3] Antennas Research Group, Austria

Abstract

The radiation characteristics of Hentenna is the objective of this paper. Furthermore, the analytical study of antenna pattern, as well as, the simulation results for both electric and electromagnetic characteristics (Input Impedance, Standing Wave Ratio SWR, Antenna Pattern and Directivity) are presented. A thorough research using 465 simulation models, in which the Hentenna's total dimension and the position of its feeding segment are the variables, proves that Hentenna is an extremely narrow band antenna. Thus, the investigation was directed not only to SWR minimalization, in terms of three most commonly used transmission lines of characteristic impedance 50-75-300 Ohm, but also to operating bandwidth improvement under an almost invariable antenna pattern. Four experimental Hentenna models were finally selected and constructed. Their antenna patterns were measured in an anechoic chamber and the measurements were found to be in good agreement with the analytical and simulated results.

Keywords

Antenna pattern, antenna analysis, antenna simulation, antenna measurements

Introduction

In 1996, Kinoshita reported that Hentenna was invented and evolved through a series of experiments carried out by Japanese radio amateurs-JE1DEU, JH1FCZ, JH1YST-during the 1970s, and he presented the Hentenna shown in Fig. 1, which is considered in this paper as the Basic Hentenna [1]. This antenna is a rectangular loop antenna having λ/6 width and λ/2 height, that is of a total length 4λ/3, and an additional, centered fed horizontal segment, the Voltage Source Segment VSS, which is positioned at a distance of λ/6 away from the short side. No-

tably, in many other references, e.g. [2], this distance equals to λ/10. According to the available information from radio amateurs, the exact position of this element is the main factor to achieve low SWR operation.

The antenna was named after the word "Hen" which, in Japanese, means "strange". Strange because, although it seems to be a vertical antenna, its polarization is horizontal.

The Hentenna was examined by the authors during an EECE diploma thesis preparation [3]. The main available tools for this study were: the antenna theory [4], the [RadPat4W] computer program for antenna patterns [5] the [RICHWIRE] simulation program [6] and the mini-Suite of software tools [7]. Since this is a plane antenna having a simple geometrical form, the analytical representation of antenna pattern, as well as the simulation and construction are all easily attainable. Moreover, its public characterization as "Miracle" wire antenna, along with the easy way of input impedance matching improvement, by moving up and down the VSS, were interesting enough reasons to check, both analytically and by simulation, the behavior of this antenna, as well as, to measure its antenna pattern.

Twenty Hentenna models were simulated by varying a) the position of VSS, and b) the total antenna length, in order to reveal and certify its rather narrow band operation. Four (4) of them were chosen to be constructed as experimental models of which the antenna pattern was measured on the three main planes xOy, yOz, zOx in anechoic chamber using the computer application ANALYZE for automated measurements developed by the Antennas Research Group, [9]. These measurements were compared with corresponding simulation output and the available analytical results [3].

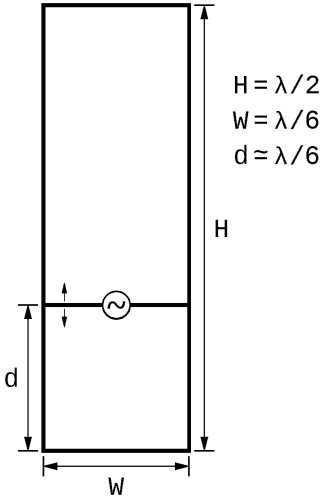

Fig. 1: The Basic Model

The first model was the Basic Hentenna [1], which we named as "B-Hentenna". The

second one was that having a Minimal SWR, "M-Hentenna". The third was selected because it had almost the same antenna pattern as the B-Hentenna but an Improved bandwidth, "I-Hentenna". And the fourth model was selected in order to highlight the great variety of Hentenna antenna patterns when the dimensions are Radically Different from those of all other publicly known Hentennas, and we named it as "W-Hentenna".

Analysis

The B-Hentenna was analytically studied considering Standing Waves SW, that is with symmetric sinusoidal current distribution:

$$\dot{I}(\ell) = \dot{I}\,\sin(\beta(h - |\ell|)), \qquad (1)$$

$$-h \leqslant \ell \leqslant +h$$

and this current (1) was used to evaluate the antenna pattern by the formulas [4]:

$$\bar{\dot{E}} = \left(\frac{1}{\lambda}\right) e^{i\beta R_k r} \dot{PF} \begin{bmatrix} \ell_\theta \\ \ell_\varphi \end{bmatrix} \qquad (2)$$

$$\dot{PF} = \int_{\ell_A}^{\ell_T} \dot{I}(\ell)\, e^{i\beta \ell_r \ell}\, d\ell \qquad (3)$$

According to the basic SW theory, on a straight wire segment of enough length, the direction of SW current remain constant over a full SW λ/2 segment, while it is opposite on either side of a SW node. These principles were applied at the Hentenna that was considered as an appropriately formed 2-wire transmission line with the shape of Square Eight SqE on which the Kirchhoff's current laws are satisfied, as shown in Fig. 2.

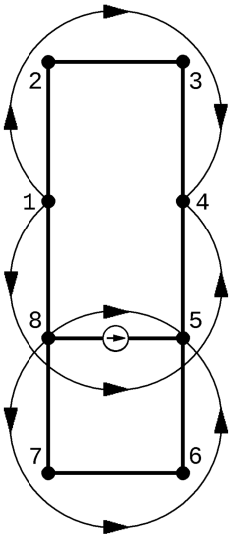

Fig. 2: Square Eight Analysis

After that we considered SqE as two square loops: the upper one is defined by points 1, 2, 3 and 4 and has a total λ length, while the lower one is defined by points 5, 6, 7, and 8 of 2λ/3 total length. On these loops the current has: 2 Full-SW currents on the upper, and 1+1/3 Full-SW currents on the lower, which

in general are different. This current arrangement results in a maximum SW antinode on the top, at the center of the segment between 2 and 3 points, as well as, on the bottom, between 7 and 6 points, respectively. Correspondingly, two overlapping SW antinodes with the same direction exist at the driving point on the VSS, between 8 and 5 points.

Thus, 4 SW currents exist, as it is shown in Fig. 2, between points: (a) 1, 2, 3 and 4, (b) 1, 8, 5 and 4, (c) 8, 7, 6 and 5, and (d) 8 and 5 where the voltage source is located. Our selection is that this (d) current has the direction of the voltage source so that the direction of all other currents result in as shown in Fig. 2, while the sum of currents on VSS is obviously SW current too. The antenna is considered on zOx plane, as it is shown in Fig. 3, in order to express $\bar{\mathbb{E}}$ using (2). We observe that, in this way, the Hentenna is analyzed as follows: three λ/2 dipoles of Π type are formed by triples of segments: (5, 1, 10), (6, 2, 9), and (7, 4, 8) and one straight line dipole of segment 3 itself, with each segment length equal to λ/6.

In Fig. 3, the arrows indicate the direction of $\vec{\ell}$ for each segment, and the dotted circles at 1, 4, 5, 8 points correspond to zero current values or current SW nodes. For each segment 1 - 10 four quantities are needed: the length of its starting point ℓ_A, the length of its end point ℓ_T, the position vector of its center $\vec{R}_k$, determined by

$$\vec{R}_{k_\nu} = \vec{OA}_\nu - \ell_{A_\nu} \vec{\ell}_\nu \qquad (4)$$

as if it was part of the corresponding line of λ/2 length, and its unit direction vector $\vec{\ell}$, with its direction to be from ℓ_A to ℓ_T in all segments. All these quantities are contained in Tab. 1a,b.

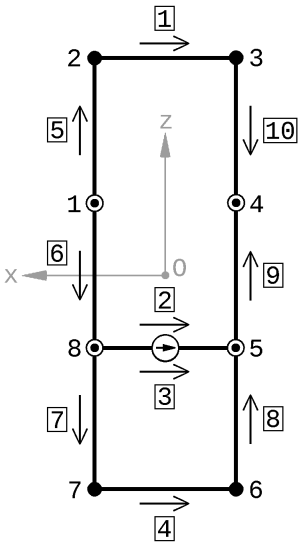

Fig. 3: 10-segment analysis

After the evaluation of the definite integral for Pattern Factor $\dot{PF}$ using (1)-(3) [3], [8], the antenna pattern of each one of the 10 segments was formulated, and by applying the law of superposition the total antenna pattern is given by

$$\bar{\mathbb{E}} = \sum_{\nu=1}^{10} \begin{bmatrix} \dot{\mathbb{E}}_{\nu\theta} \\ \dot{\mathbb{E}}_{\nu\varphi} \end{bmatrix} = \begin{bmatrix} \dot{\mathbb{E}}_{\theta} \\ \dot{\mathbb{E}}_{\varphi} \end{bmatrix} = \dot{\mathbb{E}}_{\theta}\vec{\theta}' + \dot{\mathbb{E}}_{\varphi}\vec{\varphi}' = \quad (5)$$

$$= (\mathbb{E}_{\theta_R} + i\mathbb{E}_{\theta_I})\vec{\theta}' + (\mathbb{E}_{\varphi_R} + i\mathbb{E}_{\varphi_I})\vec{\varphi}'$$

which is our working analytical expression of $\bar{\mathbb{E}}$ for the Basic B-Hentenna.

Simulation

The simulation process was carried out using the [RICHWIRE] program for the electric and electromagnetic characteristics: SWR and Input Impedance, Directivity and Antenna Pattern, in the range [900, 1300] MHz, including the chosen center operating frequency of 1111 [MHz] or $\lambda = 0.\overline{2700}$ [m], in 10 [MHz] steps, and wire radius of 1 [mm].

Fig. 4 shows the antenna pattern in the three main planes of the Basic Hentenna at 1111 [MHz], both from simulation and analysis, and it is obvious that they are in good agreement.

While these results refer to a work done back in 2004, a closer look now, 14 years later, reveals that the "strange" name given in the past to this antenna may be hidden in the form of summation (5) - but this is a subject of further investigation.

In order to simplify the geometric description of Hentenna a computer program was developed in Fortran to built the input file for [RICHWIRE] [3]. The input data were: frequency in [MHz], height and width of the outer loop in [m] and two integer values: K and N, for the number of λ/6 subdivisions of each segment and for the VSS position respectively. As the value of N increases the VSS moves up until the middle of the vertical sides due to symmetry of the antenna, and when that limit is exceeded a message appears on the screen. The numbering of points starts from VSS in order the voltage source to be always in the first segment.

The antenna wire was initially divided in λ/12 segments and then in subdivisions of λ/6. The total number of 108 segments of λ/72 length, was selected for the simulation, after investigation with 18, 36, 72, 108,

144, 180, 216, 252, 288 up to 324 segments of length λ/12, λ/24, λ/48, λ/72, λ/96, λ/120, λ/144, λ/168, λ/192, down to λ/216 respectively, because the above mentioned characteristics were almost unchanged after the 108 segments of λ/72 length.

Tab. 1a: Geometrical Data

#	ℓ_A	ℓ_T	$\vec{R}_k$		βR_{k_r}	h
			$\vec{x}'$	$\vec{z}'$		
1	$-\frac{\lambda}{12}$	$+\frac{\lambda}{12}$	0	$+\frac{\lambda}{4}$	$\frac{\pi}{2}\cos\theta$	$\frac{\lambda}{4}$
2	$-\frac{\lambda}{12}$	$+\frac{\lambda}{12}$	0	$-\frac{\lambda}{12}$	$-\frac{\pi}{6}\cos\theta$	$\frac{\lambda}{12}$
3	$-\frac{\lambda}{12}$	$+\frac{\lambda}{12}$	0	$-\frac{\lambda}{12}$	$-\frac{\pi}{6}\cos\theta$	$\frac{\lambda}{4}$
4	$-\frac{\lambda}{12}$	$+\frac{\lambda}{12}$	0	$-\frac{\lambda}{4}$	$-\frac{\pi}{2}\cos\theta$	$\frac{\lambda}{4}$
5	$-\frac{\lambda}{4}$	$-\frac{\lambda}{12}$	$+\frac{\lambda}{12}$	$+\frac{\lambda}{3}$	$\frac{\pi}{6}\sin\theta\cos\varphi+\frac{2\pi}{3}\cos\theta$	$\frac{\lambda}{4}$
6	$-\frac{\lambda}{4}$	$-\frac{\lambda}{12}$	$+\frac{\lambda}{12}$	$-\frac{\lambda}{6}$	$\frac{\pi}{6}\sin\theta\cos\varphi-\frac{\pi}{3}\cos\theta$	$\frac{\lambda}{4}$
7	$-\frac{\lambda}{4}$	$-\frac{\lambda}{12}$ *	$+\frac{\lambda}{12}$	$-\frac{\lambda}{3}$	$\frac{\pi}{6}\sin\theta\cos\varphi-\frac{2\pi}{3}\cos\theta$	$\frac{\lambda}{4}$
8	$+\frac{\lambda}{12}$	$+\frac{\lambda}{4}$	$-\frac{\lambda}{12}$	$-\frac{\lambda}{3}$	$-\frac{\pi}{6}\sin\theta\cos\varphi-\frac{2\pi}{3}\cos\theta$	$\frac{\lambda}{4}$
9	$+\frac{\lambda}{12}$	$+\frac{\lambda}{4}$	$-\frac{\lambda}{12}$	$-\frac{\lambda}{6}$	$-\frac{\pi}{6}\sin\theta\cos\varphi-\frac{\pi}{3}\cos\theta$	$\frac{\lambda}{4}$
10	$+\frac{\lambda}{12}$	$+\frac{\lambda}{4}$	$-\frac{\lambda}{12}$	$+\frac{\lambda}{3}$	$-\frac{\pi}{6}\sin\theta\cos\varphi+\frac{2\pi}{3}\cos\theta$	$\frac{\lambda}{4}$

Tab. 1b: Geometrical Data

#	$\vec{\ell}$	ℓ_r	ℓ_θ	ℓ_φ
1	$-\vec{x}$	$-\sin\theta\cos\varphi$	$-\cos\theta\cos\varphi$	$\sin\varphi$
2	$-\vec{x}$	$-\sin\theta\cos\varphi$	$-\cos\theta\cos\varphi$	$\sin\varphi$
3	$-\vec{x}$	$-\sin\theta\cos\varphi$	$-\cos\theta\cos\varphi$	$\sin\varphi$
4	$-\vec{x}$	$-\sin\theta\cos\varphi$	$-\cos\theta\cos\varphi$	$\sin\varphi$
5	$+\vec{z}$	$\cos\theta$	$-\sin\theta$	0
6	$-\vec{z}$	$-\cos\theta$	$\sin\theta$	0
7	$-\vec{z}$	$-\cos\theta$	$\sin\theta$	0
8	$+\vec{z}$	$\cos\theta$	$-\sin\theta$	0
	$+\vec{z}$	$\cos\theta$	$-\sin\theta$	0
10	$-\vec{z}$	$-\cos\theta$	$\sin\theta$	0

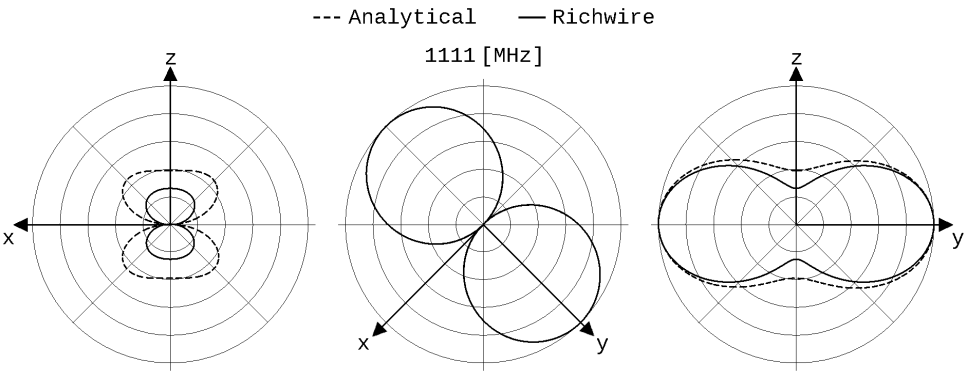

Fig. 4: Antenna patterns in 1111 [MHz] of B-Hentena

Although the B-Hentenna was designed for 1111 [MHz] operating frequency, its Standing Wave Ratio SWR shown in Fig. 5, had a minimum value at the rather distant frequency of 1260 [MHz] for a feeding line of either $Z_0 = 50$ or 75 [Ω], while its input impedance (R, X) is shown in Fig. 6. In this figure although we observe a rather wide flat of resistance $R \approx 65$ [Ω] unfortunately enough the reactance X varies almost linear with frequency in the range (–300,–100) [Ω].

After these results, the investigation focused to find the proper position of VSS in order to achieve, at least in simulation, the lowest SWR near the desired operating frequency. Thus, 18 variations of the Basic Hentenna with $H = \lambda/2$ and $W = \lambda/6$ (Fig. 1) were examined regarding the position of VSS: from λ/72 above the bottom with step λ/72, up to $18\lambda/72 = \lambda/4$ away. Fig. 7 shows six selected representative geometries where d equals to λ/72, 3λ/72, 7λ/72, $12\lambda/72 = \lambda/6$, 15λ/72 and $18\lambda/72 = \lambda/4$. The lowest value of SWR, for both 50 and 75 [Ω] line, is observed to be at $7\lambda/12 \approx \lambda/10$, that is, the same one mentioned in [2]. In Fig. 8 the corresponding antenna patterns are shown while in Fig. 9 Directivity is almost constant, changing slightly from 2.94 to 3.33 dBd. Fig. 10 shows SWR and Fig. 11 the input impedance against the distance of VSS from Hentenna's bottom.

In this way, the model with $d = 7\lambda/12$ was named M-Hentenna and was further studied. Simulation has given the SWR shown in Fig. 12 and input impedance of Fig. 13, with $R \approx 65$ [Ω] and $X \approx 0$ [Ω] at ~1111 [MHz]. The antenna pattern of M-Hentenna at 1111 [MHz] is very close to that of the B-Hentenna, as it is shown in Fig. 8. The bandwidth of this antenna, as it is defined by $SWR \leq 2$ is just ~40 [MHz], that is only ~3.5% for 50 [Ω] line and just ~50 [MHz], that is only ~4.5% for 75 [Ω] line.

Thus, the next step taken was to find a model with greater bandwidth than M-Hentenna. For this purpose, 19 different from B- and M-Hentenna models having the dimensions shown in Tab. 2 and variable VSS position were examined for minimal SWR and maximal bandwidth.

Tab. 2: 19 Hentenna models

	W				
H	λ/12	λ/6	λ/4	λ/2	λ
λ/3	v	v	v	v	v
λ/2	v	X	v	v	v
3λ/4	v	v	v	v	v
λ	v	v	v	v	v

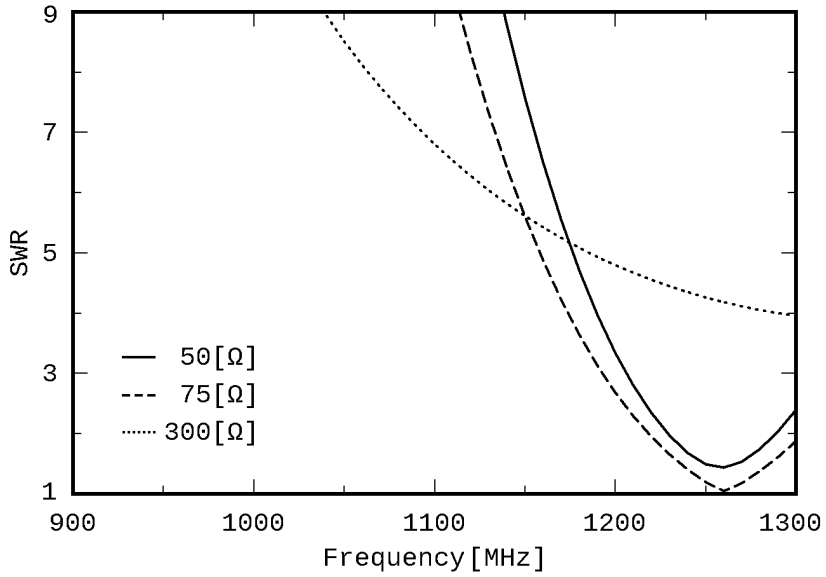

Fig. 5: SWR of B-Hentenna

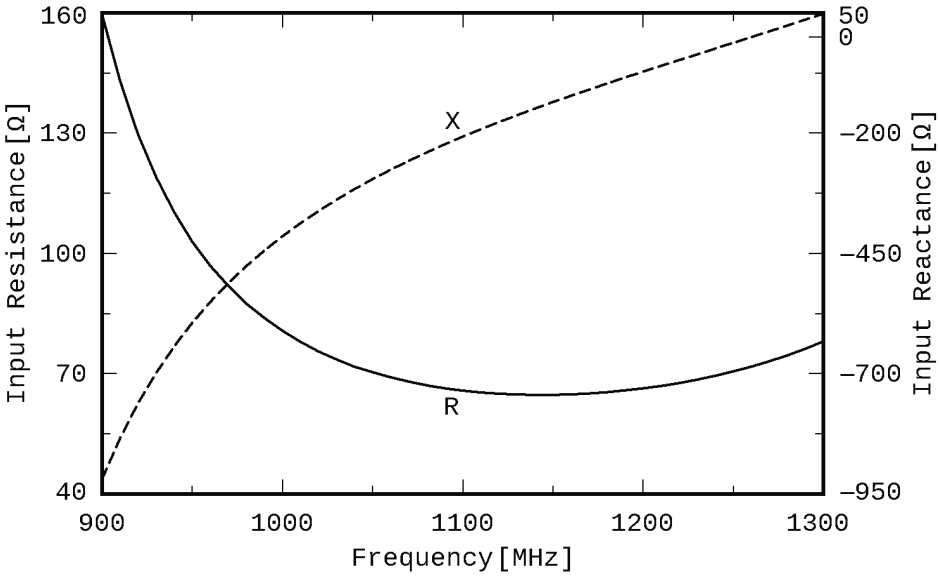

Fig. 6: Input impedance of B-Hentenna

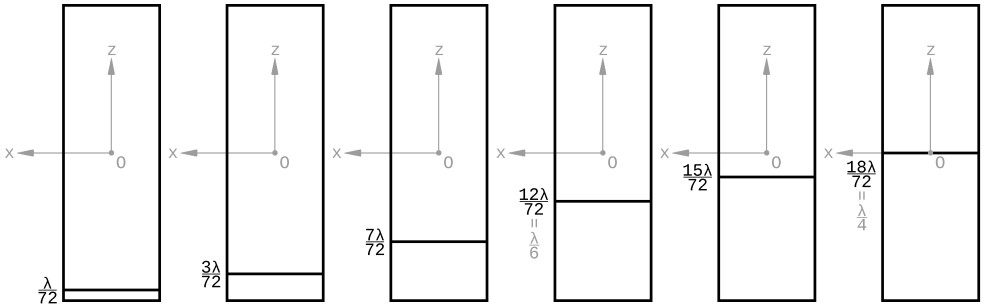

Fig. 7: VSS in various d position

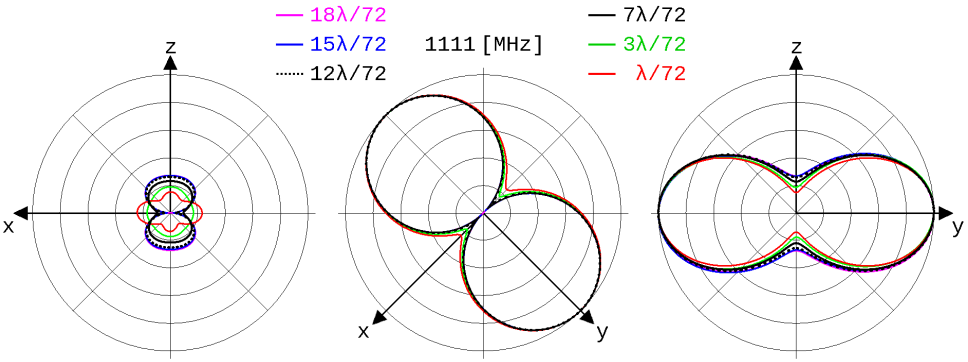

Fig. 8: Antenna patterns versus VSS position

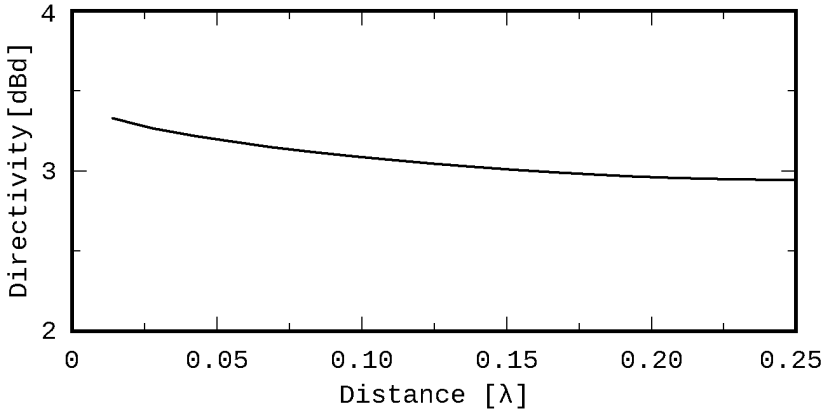

Fig. 9: Directivity versus VSS position

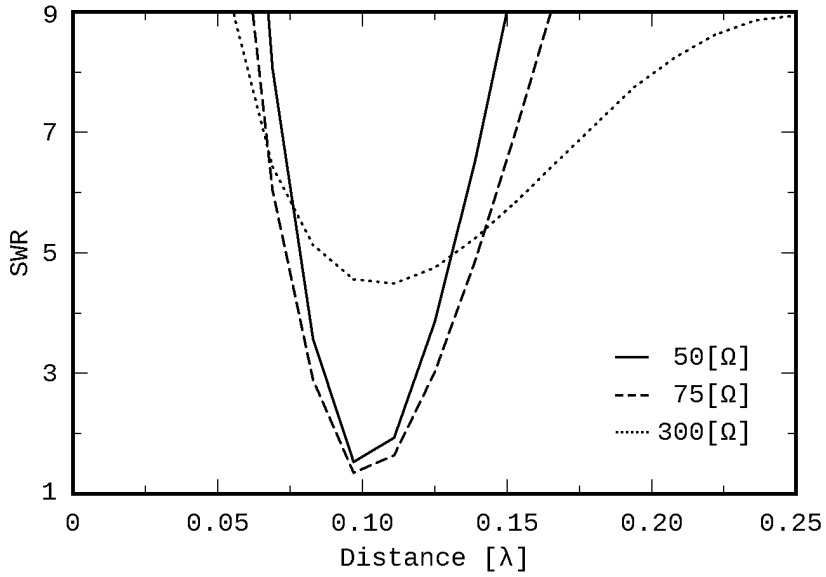

Fig. 10: SWR versus VSS position

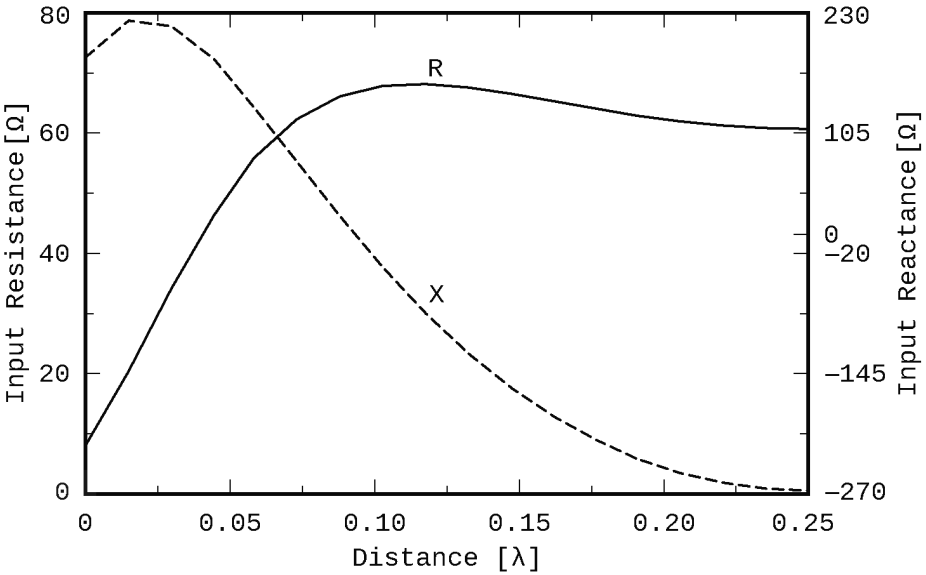

Fig. 11: Input impedance versus VSS position

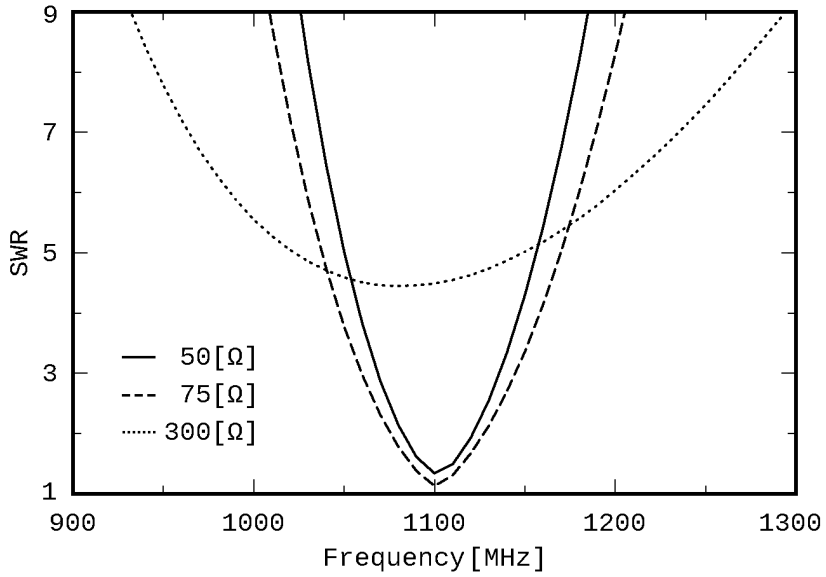

Fig. 12: SWR of M-Hentenna

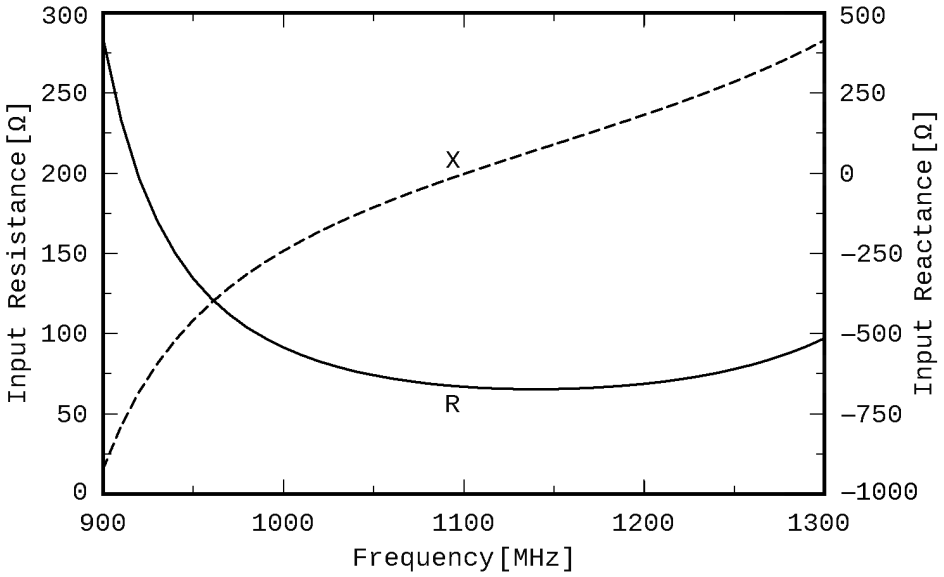

Fig. 13: Input impedance of M-Hentenna

Tab. 3 contains the extreme value of SWR for $Z_0 = 50$, 75 or 300 [Ω], and for all 20 Hentenna models $20 = 19 + 1$ in 465 arrangements with variable the VSS position d ($465 = 5 \times (12 + 18 + 27 + 36)$, where the results SWR ≤ 2 are shown with red color and their corresponding low SWR Hentennas are given in Tab. 4.

Tab. 3: Extreme values of SWR

		W									
H	Z_0 [Ω]	$\frac{\lambda}{12}$		$\frac{\lambda}{6}$		$\frac{\lambda}{4}$		$\frac{\lambda}{2}$		λ	
		Min	Max	Min	Max	Min	Max	Min	Max	Min	Max
$\frac{\lambda}{3}$	50	> 9		> 9		6.7	> 9	> 9		> 9	
	75	> 9		> 9		4.5	> 9	> 9		> 9	
	300	> 9		> 9		1.4	5.0	4.0	8.7	> 9	
$\frac{\lambda}{2}$	50	4.0	> 9	1.5	> 9	3.1	> 9	> 9		> 9	
	75	5.1	> 9	1.3	> 9	2.1	> 9	> 9		> 9	
	300	> 9		4.5	> 9	1.9	> 9	3.4	3.6	4.8	> 9
$\frac{3\lambda}{4}$	50	5.6	> 9	2.7	> 9	> 9		> 9		1.9	> 9
	75	8.3	> 9	2.8	> 9	7.5	> 9	> 9		1.3	> 9
	300	> 9		7.1	> 9	3.3	> 9	3.0	7.0	2.7	> 9
λ	50	3.9	> 9	1.2	> 9	2.7	> 9	> 9		3.5	> 9
	75	5.3	> 9	1.3	> 9	1.8	> 9	> 9		2.3	> 9
	300	> 9		4.9	> 9	2.1	> 9	3.1	4.2	1.5	> 9

Tab. 4: Low SWR Hentennas

H	W	d	Other d
λ/3	λ/4	2λ/72	
λ/2	λ/6	7λ/72:**M**	12λ/72:**B**
	λ/4	11λ/72	13λ/72:**I**
3λ/4	λ	11λ/72:**W**	
λ	λ/6	29λ/72	
	λ/4	24λ/72	
	λ	25λ/72	

In Tab. 4, the gray background indicates the Hentennas which were selected for further investigation in the frequency range [900, 1300] MHz, as well as for construction and measurement of their main-plane antenna patterns. The geometric characteristics of these four Hentennas are shown in Tab. 5.

The SWR and input impedance of these antennas are as follows:

B-Hentenna : Fig. 5, Fig. 6

M-Hentenna : Fig. 12, Fig. 13

I-Hentenna : Fig. 14, Fig. 15

W-Hentenna : Fig. 16, Fig. 17

Tab. 5: The selected Hentennas

Model	H	W	d
B-Hentenna	λ/2	λ/6	12λ/72
M-Hentenna	λ/2	λ/6	7λ/72
I-Hentenna	λ/2	λ/4	13λ/72
W-Hentenna	3λ/4	λ	11λ/72

A comparison of four Hentennas in terms of Directivity is shown in Fig. 18, in terms of SWR for 50, 75 and 300 [Ω], is shown in Figs. 19 -21 respectively, in terms of plane antenna pattern at 900, 1111 and 1300 [MHz] is shown in Fig. 22.

Finally, Fig. 23 shows the comparison of 12 twelve 3D antenna patterns in space corresponding to the four simulated Hentenna models in the above 3 three min, center and max frequencies, respectively, while Fig. 24 shows the analytical 3D antenna pattern of Basic B-Hentenna, especially.

Constructions-Measurements

The construction of the four experimental Hentenna models was made as follows.

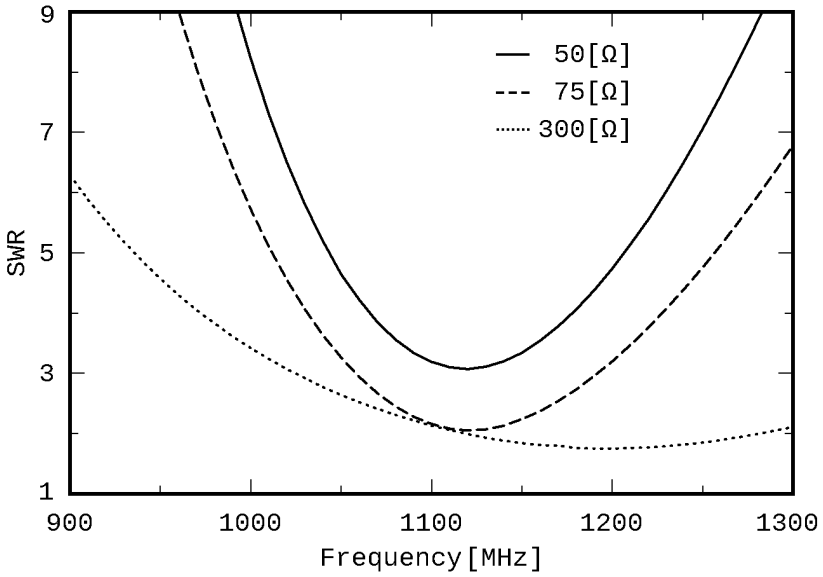

Fig. 14: SWR of I-Hentenna

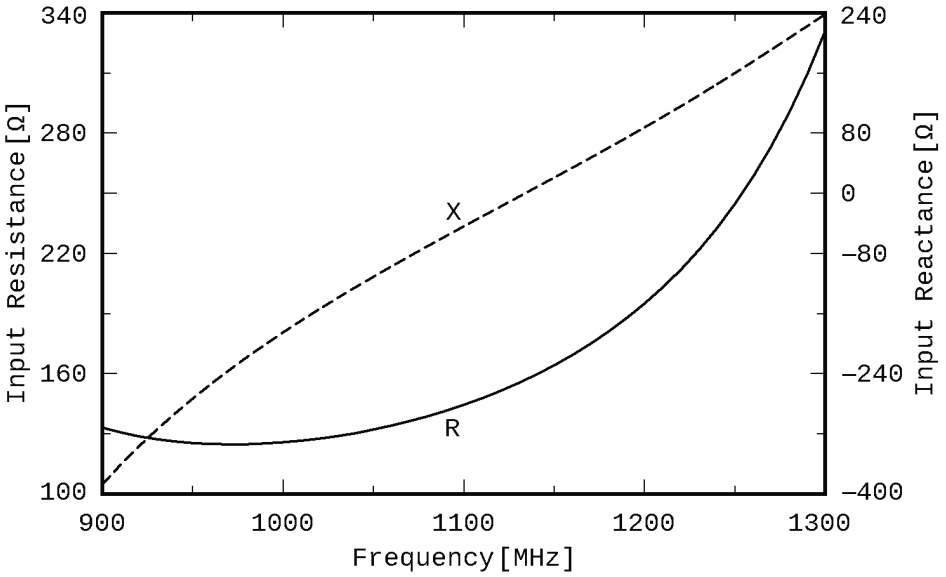

Fig. 15: Input impedance of I-Hentenna

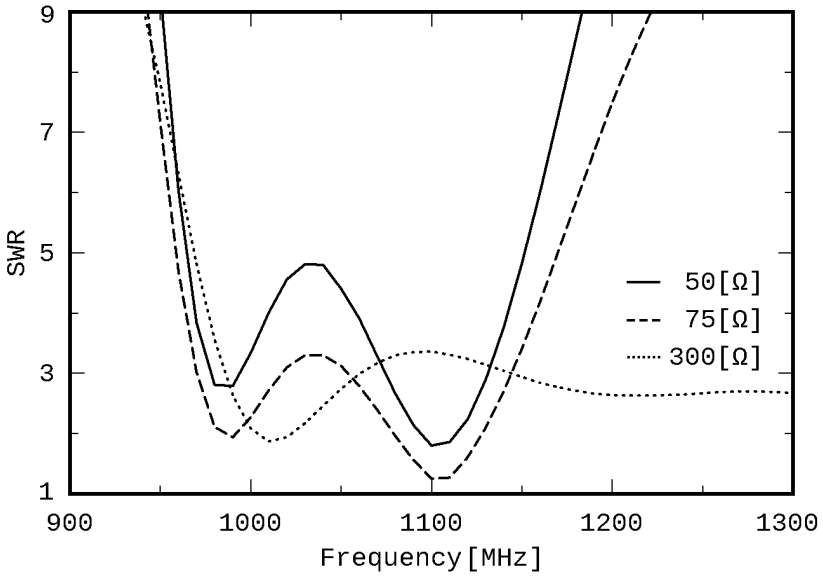

Fig. 16: SWR of W-Hentenna

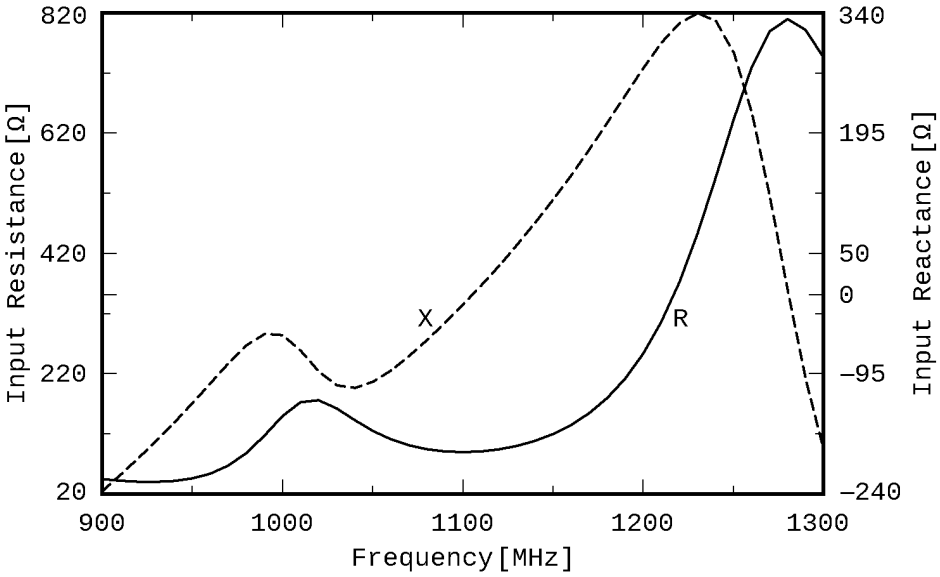

Fig. 17: Input impedance of W-Hentenna

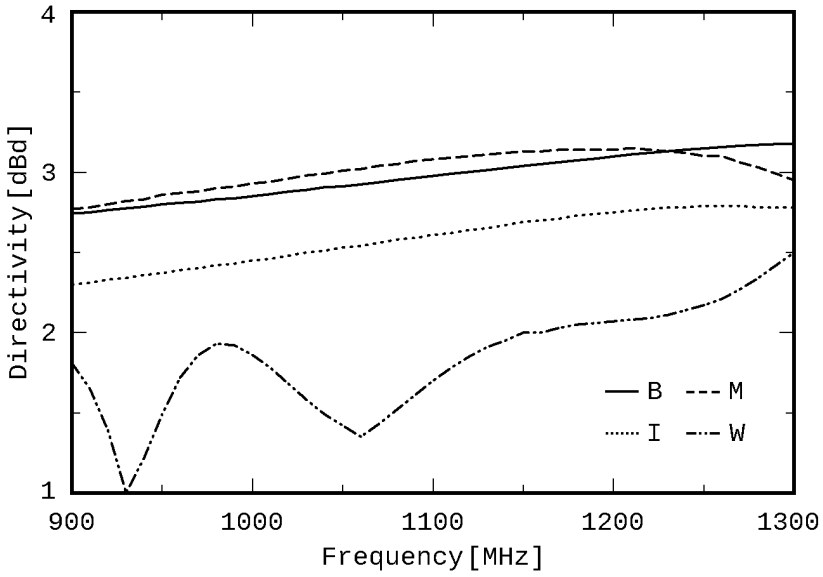

Fig. 18: Comparison of four Hentennas Directivity

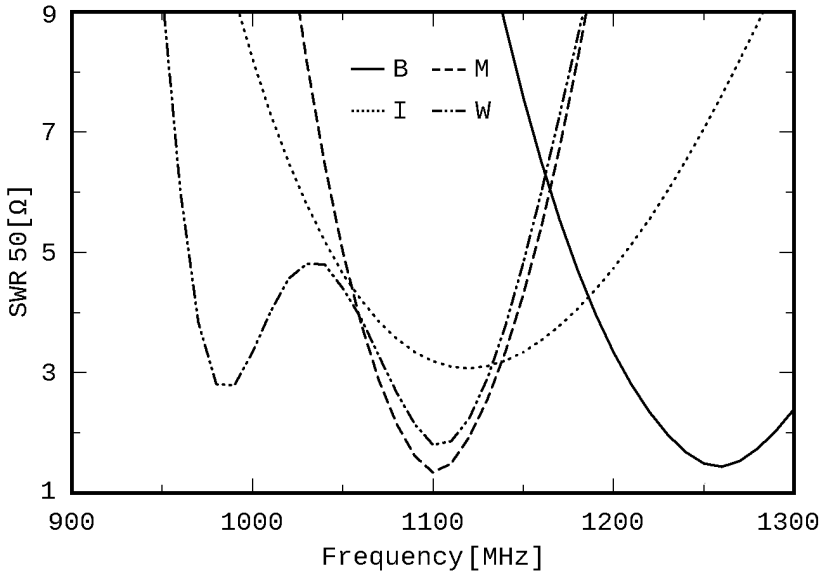

Fig. 19: Comparison of four Hentennas SWR_{50}

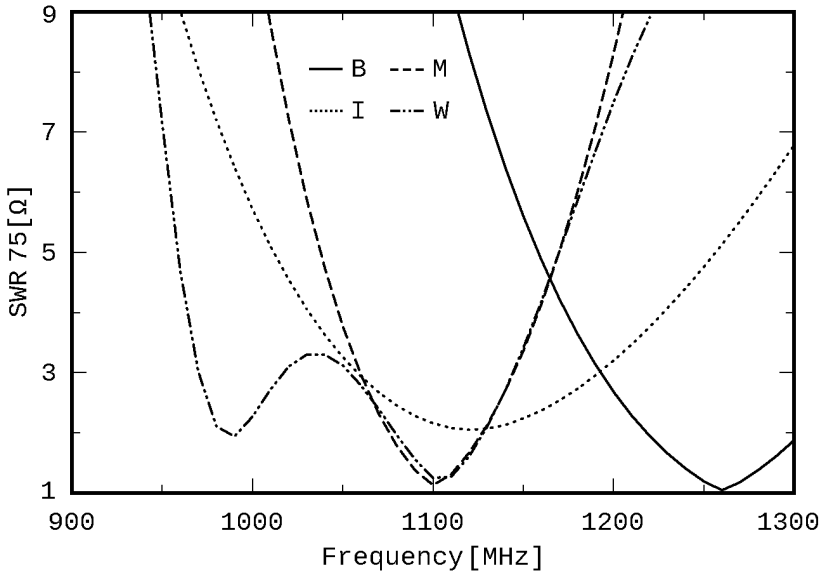

Fig. 20: Comparison of four Hentennas SWR_{75}

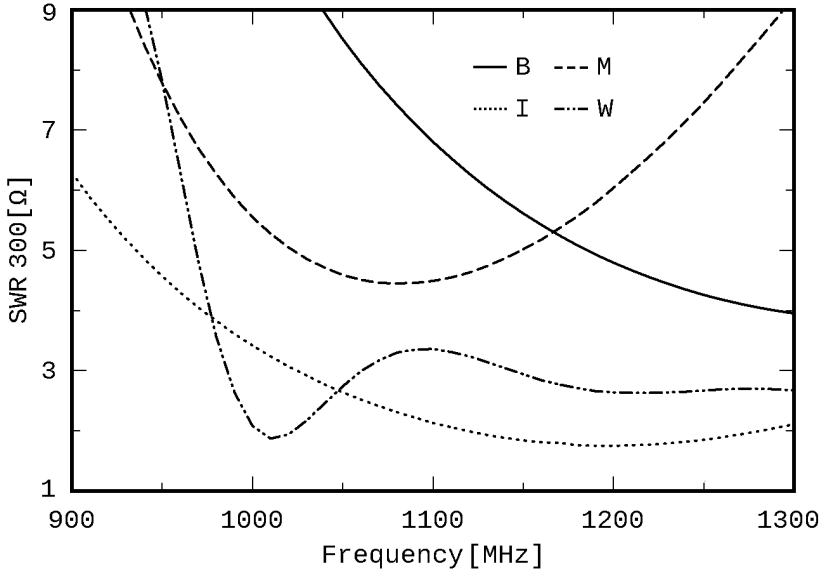

Fig. 21: Comparison of four Hentennas SWR_{300}

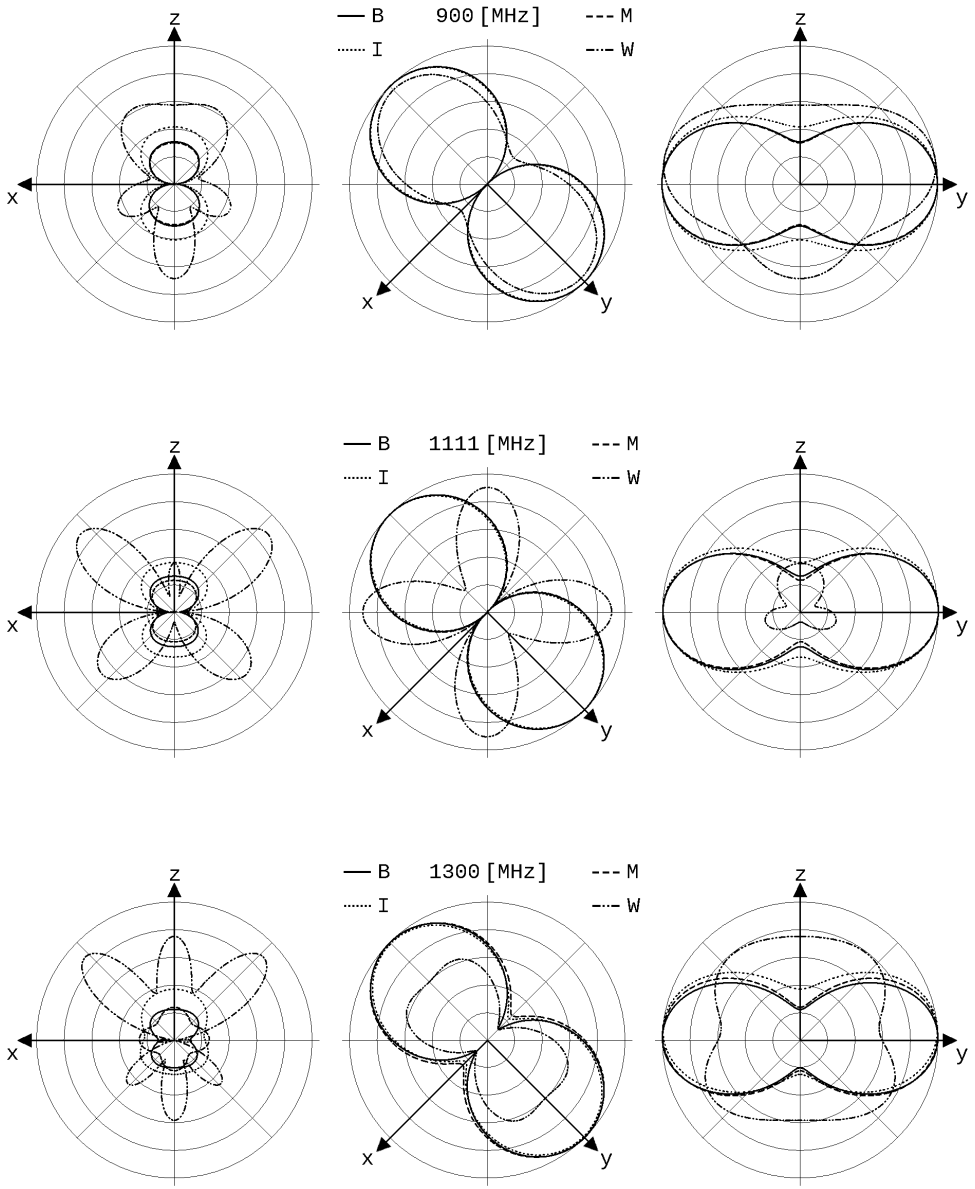

Fig. 22: Comparison of four Hentennas main-plane antenna patterns

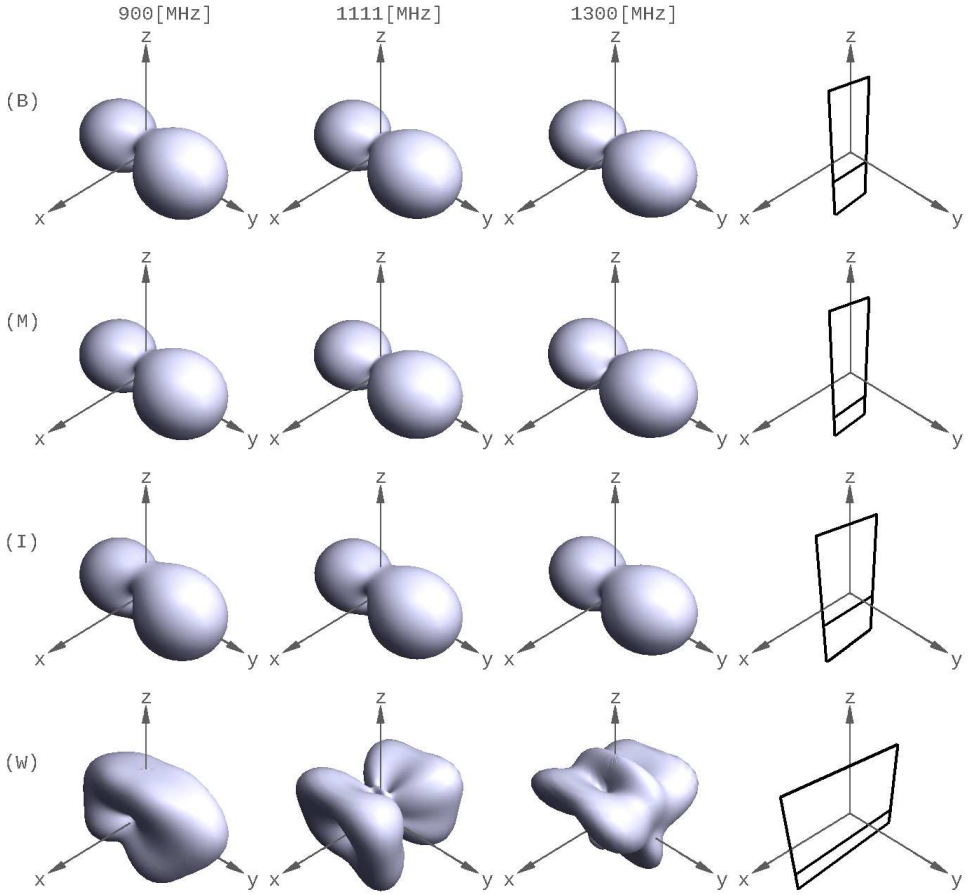

Fig. 23: Comparison of 3D antenna patterns

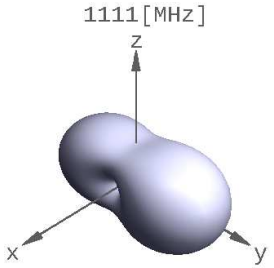

Fig. 24: 3D Analytical antenna pattern of Basic B-Hentenna

Initially, a small piece of photosensitive board was appropriately designed and printed, onto which a type-N connector, a balun, and a VSS were mounted next, in order to gradually assemble a feeding system common to all four experimental models, as shown in Fig. 25(a-j).

Since the dielectric of the connector was found to be not particularly resistive to high temperatures, that is it could be melt damaged when either of its terminals was soldered, a pin removed from an RCA male connector was used to avoid the heat destruction of dielectric. In Fig. 25(a), this pin, a female type N connector, a piece of 2.5 mm thick copper wire with adequate length, and a small piece of aluminum foil are shown. The wire was soldered in the pin and the foil covered the pin. The plastic cylindrical part of the pin was placed over them, as shown in Fig. 25(b), in order to form the hot terminal of the feeding system. Then, a ring of 1.5 mm thick copper wire, with diameter equal to the outer diameter of the connector, was constructed as shown in Fig. 25(c). On this ring, a piece of the same wire was vertically soldered, as it is shown in Fig. 25(d), and all these were fixed on the connector with its nut, as shown in Fig. 25(e), in order to form the cold terminal of the feeding system. Next, the hot terminal of Fig. 25(b) was mechanically pressed in the center pin of the connector, as shown in Fig. 25(f). Then, the balun was constructed with a $\lambda/2$ piece of coaxial cable RG-174U of $Z_0 = 50\,[\Omega]$ and velocity factor $vf = 0.66$, as it is shown in Fig. 25(g), and a piece of heat-shrinkable plastic was used to keep the balun straight in order to restrain it from disturbing the Hentennas pattern, as it is shown in Fig. 25(h). The balun and the connector terminals were soldered to the printed board in an appropriate way, that is vertically to it, as it is shown in Fig. 25(i), to complete the feeding system construction.

Next, two pieces of copper wire were also soldered in their one end on the printed board, left their other ends open, to prepare the VSS, e.g. as it is shown in Fig. 25(j) for the W-Hentenna.

Finally, the outer frame of each model was constructed and soldered to the aforementioned two open ends to finalize one-by-one the four experimental Hentennas shown in Fig. 26.

Fig. 25: VSS and Balun

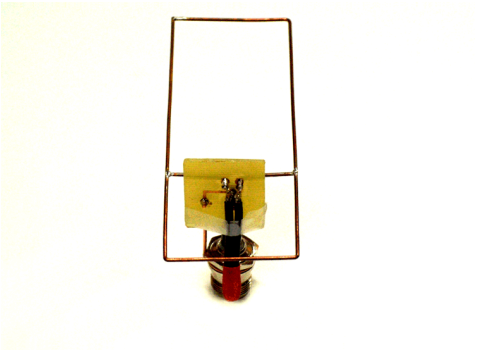

B-Hentenna

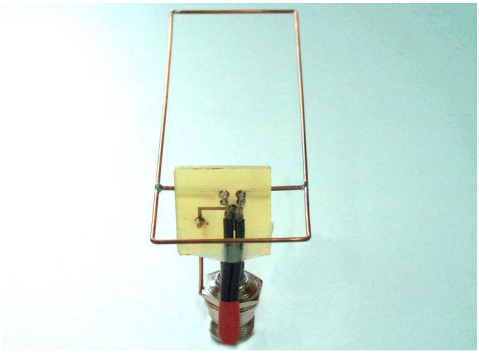

M-Hentenna

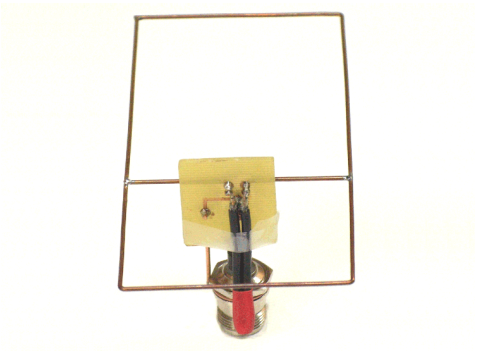

I-Hentenna

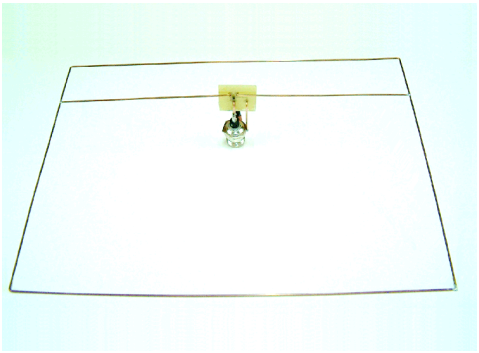

W-Hentenna

Fig. 26: Experimental Hentenna models

The measurement system was consisted of a 50 [Ω] Vector Network Analyzer external to an anechoic chamber [10]. Each Hentenna under test was appropriately positioned as a receiving antenna three times. Each time was azimuthally rotated around one of its three main-axes, by using a built 360° hardware developed positioner, which was software controlled by a developed program. The stationary transmitting source was a UHF standard gain antenna [11].

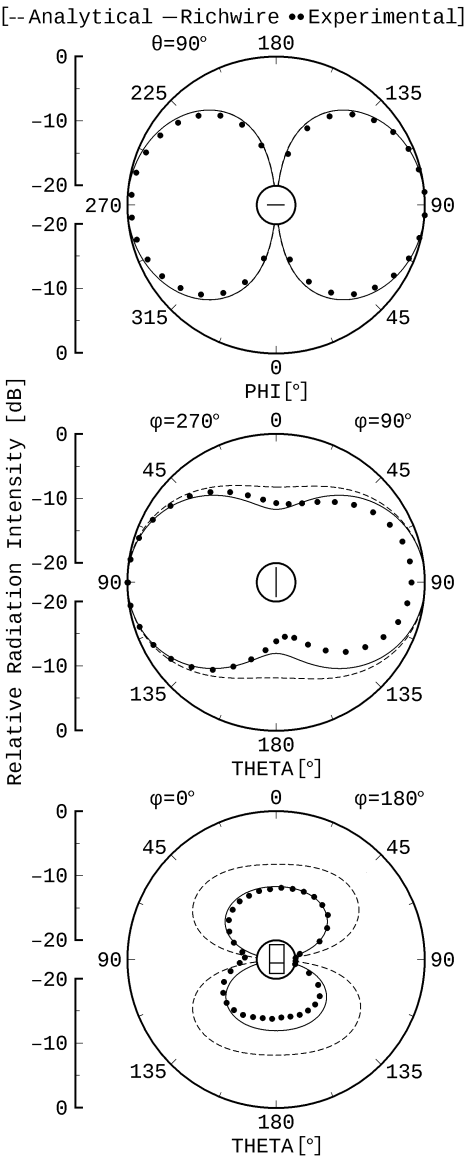

Fig. 27: Analysis, simulation, measurements of B-Hentenna: H = λ/2, W = λ/6, d = λ/6

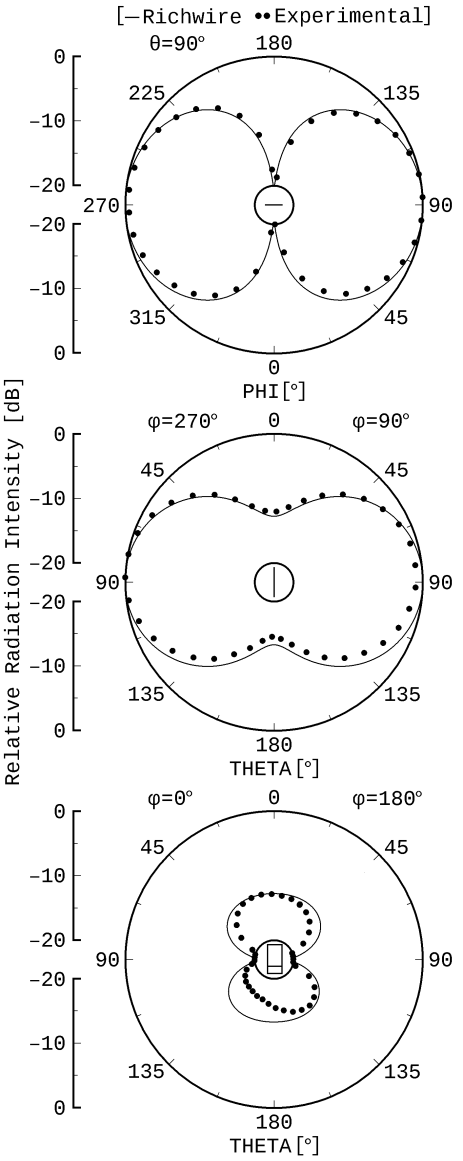

Fig. 28: Analysis, simulation, measurements of M-Hentenna: H = λ/2, W = λ/6, d = λ/10

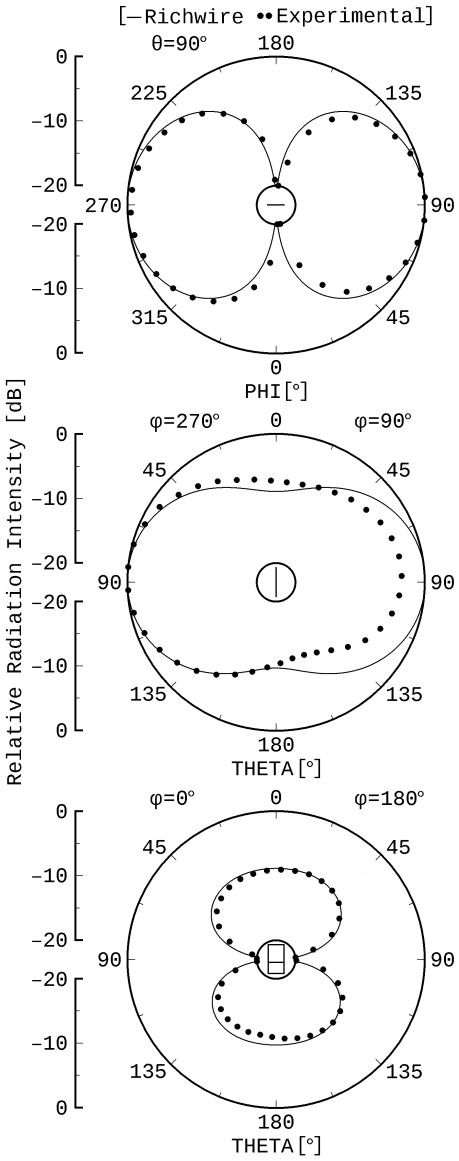

Fig. 29: Analysis, simulation, measurements of I-Hentenna: H = λ/2, W = λ/4, d = 13λ/72

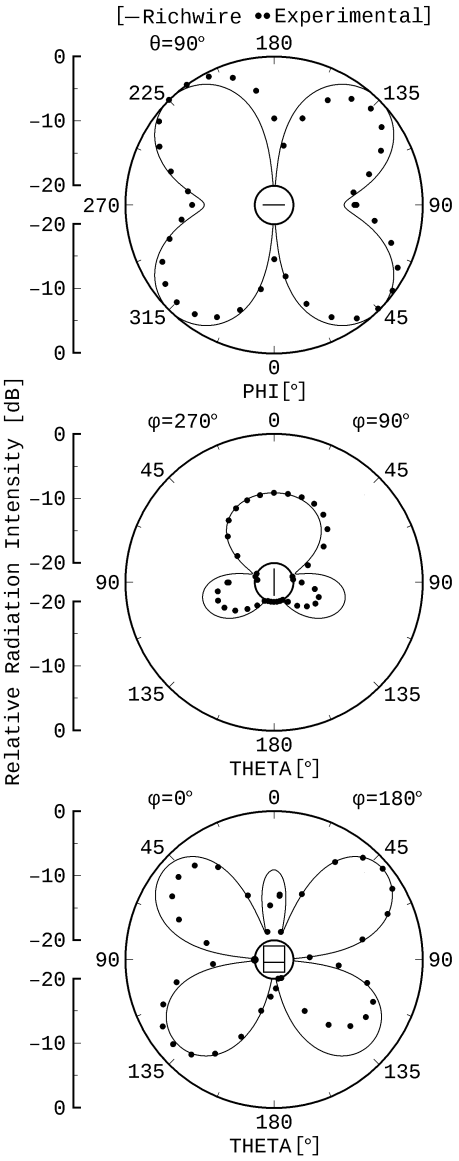

Fig. 30: Analysis, simulation, measurements of W-Hentenna: H = 3λ/4, W = λ, d = 11λ/72

Fig. 27 illustrates the measurements of radiation intensity $\mathcal{U} = \mathcal{E}^2$ in [dB] on the three main-planes for the Basic B-Hentenna, along with the corresponding results from analysis and simulation at the center operating frequency of 1111 [MHz]. In Figs. 28, 29, and 30, a comparison of simulation and measurement results are shown for the experimental M-, I- and W-Hentenna, respectively. Obviously, a very good agreement in all planes was achieved, even for the wide W-Hentenna, which had a strongly different antenna pattern.

In Tab. 6 the main characteristics of these four Hentenna types are reducibly shown to the operating wavelength λ and by using systematic approximation as follows:

If $0 \le r$ is a result, with $I = [r]$ and $F = \{r\}$ to be the Integer and Fractional parts of it respectively, where $I, F \in \mathbb{N} \cup \{0\}$ and $0.F \in [0, 1)$, as well as, $I' = [r']$ and $F' = \{r'\}$ similarly are the corresponding parts of its systematic rounding $r' = I'.F'$, then our rounding to the tenths, is of the type "to the nearest", and it is taken place according to the following scheme:

(1): $0.F \in [0\ \ , 0.25) \Rightarrow F' = 0 \wedge I' = I$

(2): $0.F \in [0.25, 0.75) \Rightarrow F' = 5 \wedge I' = I$

(3): $0.F \in [0.75, 1\ \ ) \Rightarrow F' = 0 \wedge I' = I + 1$

Tab. 6: Hentenna Types

	B-Basic	M-Minimal SWR	I-Improved BW	W-Wide
H [λ]	1/2	1/2	1/2	3/4
W [λ]	1/6	1/6	1/4	1
d [λ]	12/72	7/72	13/72	11/72
D [dB_d]	3	3	2.5	2
SWR_{50} – BW %	13 – 5	1.5 – 3.5	3	2 – 2
SWR_{75} – BW %	9.5 – 6.5	1.5 – 4.5	2	1.5 – 4.5
SWR_{300} – BW %	6	4.5	2 – 13.5	3.5 – 2

Conclusion

The fact that, although we applied the proposed formulas [1] to study a Basic B-Hentenna for operation at 1111 [MHz] we got the lowest SWR nearly to the rather distant frequency of 1260 [MHz], lead us to search a more appropriate position of the Voltage Source Segment VSS in order to low the SWR closely to operating frequency, and it was this investigation that resulted the Minimal SWR M-Hentenna.

After that, to further improve the Hentenna characteristics, 465 different models of it were simulated, from which an Hentenna of improved bandwidth, I-Hentenna resulted.

Finally, one additional Hentenna was selected out from 465 models which it was wider both in height and width than the three previous models, in order to study a radically different antenna pattern, the W-Hentenna.

From Tab. 6, M-Hentenna indeed possess the well known in radio amateur cycles 3 dB_d Directivity and the lowest SWR_{50}, while I-Hentenna has the largest BW but with a minimum value of SWR_{300} at 1200 [MHz].

Corresponding to these Hentenna types four experimental models were constructed and their main-plane antenna patterns were measured in an anechoic chamber at the center operating frequency of 1111 [MHz]. These measurements were found in good agreement with the prediction results form analysis and simulation.

During this past Hentenna study [3], we provoked a related discussion at the rec. radio.amateur.antenna newsgroup of usenet [12], in order to collect various comments regarding unpredicted aspects of this subject.

The impression made out of the contributors' remarks was that further research, concerning mainly the analytical determination of the antenna pattern, is needed and thus this work was planned to be one of the authors' future activities.

References

[1] Kinoshita S., "The Hentenna-The Japanese 'Miracle' Wire Antenna", ARRL, "The ARRL Antenna Compendium Vol.5", 1996, pp. 66-68.

[2] Radio Amateur jr1lzk, "Introduction of Hentenna", http://www.ve3sqb.com/hamaerials/jr1lzk/

[3] Babli E., "The Hentenna", Diploma Thesis #31, ARG—Antennas Research Group, DUTh, 2004 (in Hellenic)
https://www.antennas.gr/theses/diploma/dt31-hkh.pdf

[4] Zimourtopoulos P., "Antenna Notes 1999-, Antenna Design Notes 2000-",(in Hellenic)
https://www.antennas.gr/antennanotes/

[5] Yannopoulou N.I., Zimourtopoulos P.E., "Antenna Radiation Patterns: RadPat4W — FLOSS for MS Windows or Wine Linux", FunkTechnikPlus # Journal, Issue 5, Year 2, 2014, pp. 33-45
https://www.otoiser.org/index.php/ftpj/article/download/47/42

[6] Richmond J.H., "Computer program for thin-wire structures in a homogeneous conducting medium", Publication Year: 1974, NTRS-Report/Patent Number: NASA-CR-2399, ESL-2902-12, DocumentID: 19740020595,
https://ntrs.nasa.gov/search.jsp?R=19740020595

[7] Yannopoulou N., Zimourtopoulos P., "Mini Suite of Antenna Tools, Educational Laboratories, Antennas Research Group, 2006,
https://www.antennas.gr/antsoft/minisuiteoftools/

[8] Yannopoulou N.I., "Study of monopole antennas over a multi-frequency decoupling cylinder", PhD Thesis, EECE, DUTh, February 2008 (in Hellenic), pp. (2-6)-(2-9)
https://www.didaktorika.gr/eadd/handle/10442/20920?locale=en

[9] Yannopoulou N., Zimourtopoulos P., "ANALYZE: Automated Antenna Measurements, ver. 13", Antennas Research Group, 1993-2008

[10] Yannopoulou N., Zimourtopoulos P., "Total Differential Errors in One Port Network Analyzer Measurements with Application to Antenna Impedance", Radioengineering, Vol. 16, No. 2, June 2007, pp. 1-8
https://www.radioeng.cz/fulltexts/2007/07_02_01_08.pdf

[11] Yang R.F.H., "A proposed gain standard for VHF antennas", IEEE Transactions on Antennas and Propagation, 1966, Vol. 14, No. 6, p. 792

[12] Babli E. as "emma", et. al., "Constructional details", rec.radio.amateur.antenna, USENET, 10.11.2003-9.12.2003+
https://groups.google.com/d/msg/rec.radio.amateur.antenna/9UttkZLOH5w/4iYbMwsgKLgJ

* Active Links: 27.11.2018

Previous Publication in FUNKTECHNIKPLUS # JOURNAL

"Measurement Uncertainty in Network Analyzers:
Differential Error Analysis of Error Models Part 4:
Non-Zero Length Through in Full Two-Port SLOT Calibration"
Issue 11, Year 4, pp. 7-29

*** About The Authors**

Babli Eleni, was born in Alexandroupoli, Evros, Greece in 1980. She graduated from Electrical Engineering and Computer Engineering in 2004 from Democritus University of Thrace, Xanthi, Greece. Member of Antennas Research Group while she was elaborated her diploma thesis. She received her Msc in MBA-TQM in 2006 from University of Piraeus, Department of Organization and Business Administration and the Pedagogical Education Certificate in 2012 from School of Pedagogical and Technological Education. She worked as Business Consultant & Quality Assurance Manager for Innovatia LTD in 2006-2010 and for Orion Consulting in 2010-2015 and as Teacher of Computer Science in technical schools, 2010-. Currently she is a student in School of Pharmacy, Aristotle University of Thessaloniki.

ebabli@yahoo.com

Nikolitsa Yannopoulou, Issue 9, Year 3, p. 390

yin@arg.op4.eu

Petros Zimourtopoulos, Issue 9, Year 3, p. 390

pez@arg.op4.eu